Eur. Phys. J. D **31**, 131–135 (2004)
DOI: 10.1140/epjd/e2004-00113-4

THE EUROPEAN PHYSICAL JOURNAL D

Phase diagram for the Grover algorithm with static imperfections

A.A. Pomeransky[1], O.V. Zhirov[2], and D.L. Shepelyansky[1,a]

[1] Laboratoire de Physique Théorique, UMR 5152 du CNRS, Université P. Sabatier, 31062 Toulouse Cedex 4, France
[2] Budker Institute of Nuclear Physics, 630090 Novosibirsk, Russia

Received 3 May 2004 / Received in final form 1st July 2004
Published online 31 August 2004 –

Abstract. We study effects of static inter-qubit interactions on the stability of the Grover quantum search algorithm. Our numerical and analytical results show existence of regular and chaotic phases depending on the imperfection strength ε. The critical border ε_c between two phases drops polynomially with the number of qubits n_q as $\varepsilon_c \sim n_q^{-3/2}$. In the regular phase ($\varepsilon < \varepsilon_c$) the algorithm remains robust against imperfections showing the efficiency gain $\varepsilon_c/\varepsilon$ for $\varepsilon \gtrsim 2^{-n_q/2}$. In the chaotic phase ($\varepsilon > \varepsilon_c$) the algorithm is completely destroyed.

PACS. 03.67.Lx Quantum Computation – 24.10.Cn Many-body theory – 73.43.Nq Quantum phase transitions

Quantum computations open new perspectives and possibilities for treatment of complex computational problems in a more efficient way with respect to algorithms based on the classical logic [1]. In the quantum computers classical bits are replaced by two-level quantum systems (qubits) and classical operations with bits are substituted by elementary unitary transformations (quantum gates). The elementary gates can be reduced to single qubit rotations and controlled two-qubit operations, e.g. *control-NOT* gate [1]. Combinations of elementary gates allow to implement any unitary operation on a quantum register, which for n_q qubits contains exponentially many states $N = 2^{n_q}$. The two most famous quantum algorithms are the Shor algorithm for integer number factorization [2] and the Grover quantum search algorithm [3]. The Shor algorithm is exponentially faster than any known classical algorithm, while the Grover algorithm gives a quadratic speedup.

In realistic quantum computations the elementary gates are never perfect and therefore it is very important to analyze the effects of imperfections and quantum errors on the algorithm accuracy. A usual model of quantum errors assumes that angles of unitary rotations fluctuates randomly in time for any qubit in some small interval ε near the exact angle values determined by the ideal algorithm. In this case a realistic quantum computation remains close to the ideal one up to a number of performed gates $N_g \sim 1/\varepsilon^2$. For example, the fidelity f of computation, defined as a square of scalar product of quantum wavefunctions of ideal and perturbed algorithms, remains close to unity if a number of performed gates is smaller than N_g. This result has been established analytically and numerically in extensive studies of various quantum algorithms [4–10].

Another source of quantum errors comes from internal imperfections generated by residual static couplings between qubits and one-qubit energy level shifts which fluctuate from one qubit to another but remain static in time. These static imperfections may lead to appearance of many-body quantum chaos, which modifies strongly the hardware properties of realistic quantum computer [11–13]. The effects of static imperfections on the accuracy of quantum computation have been investigated on the examples of quantum algorithms for the models of complex quantum dynamics [8,10,14,15]. As a result a universal law for fidelity decay induced by static imperfections has been established [10] for quantum algorithms simulating dynamics in the regime of quantum chaos. At the same time it has been realized that the effects of static imperfections for dynamics in an integrable regime are not universal and more complicated. Therefore it is important to investigate the effects of static imperfections on an example of the well-known Grover algorithm. First attempt was done recently in [16], but the global picture of the phenomenon remained unclear. In this paper we present extensive numerical and analytical studies which establish the global stability diagram of reliable operability of the Grover algorithm.

Let us first outline the key features of the Grover algorithm [3]. An unstructured database is presented by $N = 2^{n_q}$ states of quantum register with n_q qubits: $\{|x\rangle\}$, $x = 0, \ldots, N-1$. The searched state $|\tau\rangle$ can be identified by *oracle* function $g(x)$, defined as $g(x) = 1$ if $x = \tau$ and $g(x) = 0$ otherwise. The Grover iteration operator $\hat{G}$

[a] e-mail: dima@irsamc.ups-tlse.fr

is a product of two operators: $\hat{G} = \hat{D}\hat{O}$. Here the oracle operator $\hat{O} = (-1)^{g(\hat{x})}$ is specific to the searched state $|\tau\rangle$, while the diffusion operator $\hat{D}$ is independent of $|\tau\rangle$: $D_{ii} = -1 + 2/N$ and $D_{ij} = 2/N$ $(i \neq j)$. For the initial state $|\psi_0\rangle = \sum_{x=0}^{N-1} |x\rangle/\sqrt{N}$, t applications of the Grover operator $\hat{G}$ give [1]:

$$|\psi(t)\rangle = \hat{G}^t|\psi_0\rangle = \sin\left((t+1/2)\omega_G\right)|\tau\rangle + \cos\left((t+1/2)\omega_G\right)|\eta\rangle \quad (1)$$

where the Grover frequency $\omega_G = 2\arcsin(\sqrt{1/N})$ and $|\eta\rangle = \sum_{x\neq\tau}^{(0\leq x<N)} |x\rangle/\sqrt{N-1}$. Hence, the ideal algorithm gives a rotation in the 2D plane $(|\tau\rangle, |\eta\rangle)$.

The implementation of the operator D through the elementary gates requires an ancilla qubit. As a result the Hilbert space becomes a sum of two subspaces $\{|x\rangle\}$ and $\{|x+N\rangle\}$, which differ only by a value of (n_q+1)th qubit. These subspaces are invariant with respect to operators O and D: $O = 1 - 2|\tau\rangle\langle\tau| - 2|\tau+N\rangle\langle\tau+N|$, $D = 1 - 2|\psi_0\rangle\langle\psi_0| - 2|\psi_1\rangle\langle\psi_1|$, where $|\psi_1\rangle = \sum_{x=0}^{N-1} |x+N\rangle/\sqrt{N}$ and $|\psi_{0,1}\rangle$ correspond to up/down ancilla states. Then D can be represented as $D = WRW$ [3], where the transformation $W = W_{n_q} \ldots W_k \ldots W_1$ is composed from n_q one-qubit Hadamard gates W_k, and R is the n_q-controlled phase shift defined as $R_{ij} = 0$ if $i \neq j$, $R_{00} = 1$ and $R_{ii} = -1$ if $i \neq 0$ $(i,j = 0,\ldots,N-1)$. In turn, this operator can be represented as $R = W_{n_q}\sigma^x_{n_q-1}\ldots\sigma^x_1 \wedge_{n_q} \sigma^x_{n_q-1}\ldots\sigma^x_1 W_{n_q}$, where $\wedge_{n_q}$ is generalized n_q-qubit Toffolli gate, which inverts the n_qth qubit if the first n_q-1 qubits are in the state $|1\rangle$. The construction of $\wedge_{n_q}$ from 3-qubit Toffolli gates with the help of only one auxiliary qubit is described in [17]. As a result the Grover operator G is implemented through $n_g = 12n_{tot} - 42$ elementary gates including one-qubit rotations, control-NOT and Toffolli gates. Here $n_{tot} = n_q + 1$ is the total number of qubits.

To study effects of static imperfections on the Grover algorithm we use the model introduced in [11]. In this model a quantum computer hardware is described by the Hamiltonian H:

$$H = \sum_i \frac{\Delta}{2}\sigma_i^z + H_S, \quad H_S = \sum_i a_i\sigma_i^z + \sum_{i<j} b_{ij}\sigma_i^x\sigma_j^x. \quad (2)$$

Here, σ_i are the Pauli matrices for qubits i, and Δ is an average one-qubit energy spacing. All n_{tot} qubits are placed on a rectangular lattice, the second sum in H_S runs over nearest neighbor qubits with periodic boundary conditions. Qubit energy shifts a_i and couplings b_{ij} are randomly and uniformly distributed in the intervals $[-\alpha,\alpha]$ and $[-\beta,\beta]$, respectively. Following [8,10,14,15] we assume that the average spacing Δ is compensated by specially applied laser pulses so that between subsequent elementary gates the wavefunction evolution is given by the propagator $U_S = \exp(-iH_S t_g)$. Thus all static errors are expressed via this propagator while the elementary gates are taken to be perfect. Appropriate rescaling of parameters a_i and b_{ij} allows to put $t_g = 1$ without any loss of generality. We concentrate our studies on the case $\alpha = \beta \equiv \varepsilon$ where inter-qubit couplings lead to a developed quantum chaos [11,14].

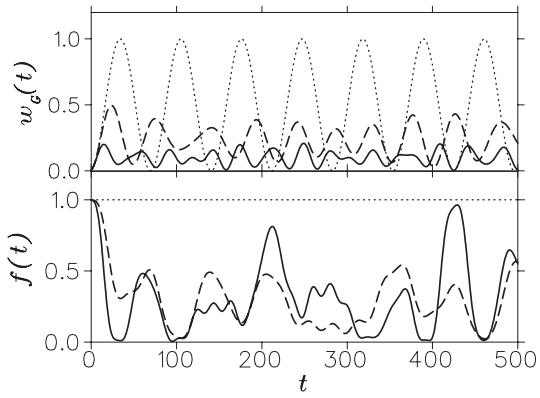

Fig. 1. Probability of searched state $w_G(t)$ (top) and fidelity $f(t)$ (bottom) as a function of the iteration step t in the Grover algorithm for $n_{tot} = 12$ qubits. Dotted curves show results for the ideal algorithm ($\varepsilon = 0$), dashed and solid curves correspond to imperfection strength $\varepsilon = 4 \times 10^{-4}$ and 10^{-3}, respectively.

A typical example of imperfection effects on the accuracy of the Grover algorithm is shown in Figure 1 for a fixed disorder realization of H_S in (2) on 3×4 qubit lattice. It clearly shows that imperfections suppress the probability w_G to find the searched state, where w_G is given by a sum of probabilities of states $|\tau\rangle$ and $|\tau+N\rangle$. In contrast to the case of time-dependent random quantum errors studied in [7] in the case of static imperfections the oscillations of probability w_G do not decrease with time t. Another interesting feature is a significant decrease of the period of the Grover oscillations compared to the case of ideal algorithm, where $T_G = \pi/2\omega_G$. This effect is also absent in the case of random errors. The fidelity of quantum computation $f(t)$ also shows non-decaying oscillations at large times. However, in average the maxima of fidelity correspond to minima rather than maxima of probability w_G. Hence, $f(t)$ is not appropriate for tests of the algorithm accuracy. The physical reason for this unusual situation is related to the fact that when $w_G \approx 0$ all probability is concentrated in one initial state even for relatively large perturbation (see Fig. 2 and discussion below) and therefore the fidelity becomes close to unity. However, at such moments it is not possible to detect the searched state.

Following [18] a pictorial presentation of the dynamical evolution in the Grover algorithm can be obtained with the help of the Husimi function [19], which is shown in Figure 2. In this presentation the computational basis x can be considered as a coordinate space representation for the wavefunction $\psi_x(t)$ $(x = 0,\ldots,2N-1)$, while the conjugated basis obtained by the Fourier transform corresponds to momentum representation p $(p = -N+1,\ldots,N)$. In this way the initial state of the Grover algorithm $|\psi_0\rangle$ gives a peaked distribution with $p = 0$. In the ideal algorithm the total probability is distributed between two states $|\tau\rangle$ and $|\eta\rangle$ (see Eq. (1)) that gives two orthogonal lines in the phase space of Husimi function (see Fig. 2, top raw). After the period $T_G \approx 34$ all the probability is transferred to

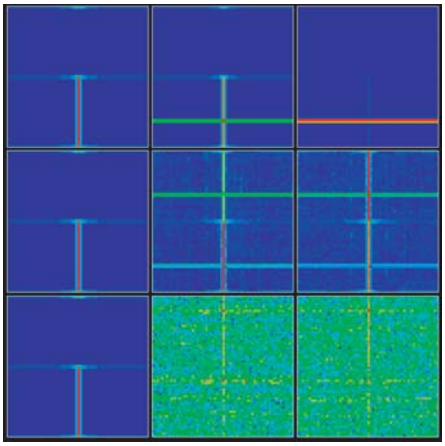

Fig. 2. Evolution of the Husimi function in the Grover algorithm at times $t = 0$, 17, and 34 (from left to right), and for $\varepsilon = 0$, 0.001, and 0.008 (from top to bottom). The qubit lattice and disorder realization are the same as in Figure 1. The vertical axis shows the computational basis $x = 0, \ldots, 2N-1$, while the horizontal axis represents the conjugated momentum basis. Density is proportional to color changing from maximum (red) to zero (blue). A color version is available online at `http://www.eurphysj.org`.

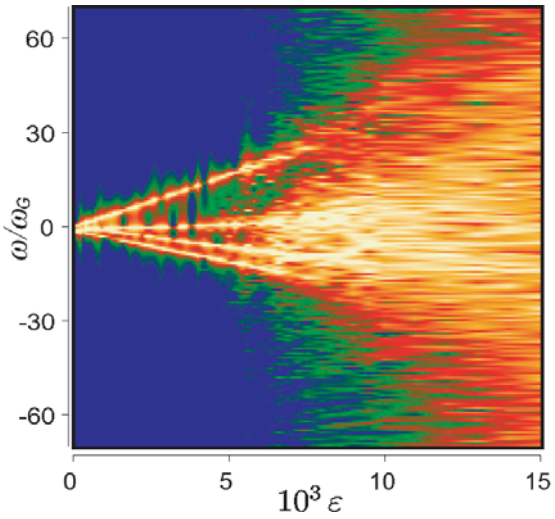

Fig. 3. Phase diagram for the spectral density $S(\omega)$ as a function of imperfection strength ε, $n_{tot} = 12$, same disorder realization as in Figure 2. Color is proportional to density $S(\omega)$ (yellow for maximum and blue for zero). A color version is available online at `http://www.eurphysj.org`.

the target state $|\tau\rangle$ ($w_G \approx 1$). In the presence of moderate imperfections the flips of the ancilla qubit become possible that involves into dynamics two additional states. As a result the probability is mainly distributed over *four states* corresponding to four straight lines in phase space (Fig. 2, middle raw):

$$|\tau_0\rangle = |\tau\rangle \quad |\tau_1\rangle = |\tau + N\rangle$$

$$|\eta_0\rangle = |\eta\rangle \quad |\eta_1\rangle = \sum_{x\neq\tau}^{(0\leq x<N)} |x+N\rangle/\sqrt{N-1}. \qquad (3)$$

The probability w_4 contained in these states is close to unity (in Fig. 2 $w_4 = 0.998$ for $\varepsilon = 10^{-3}$). Above certain critical border ε_c this simple structure is completely washed out ($w_4 = 6 \times 10^{-4}$), and the Husimi function shows only random distribution (Fig. 2, bottom raw).

The dominant contribution of these four states can be also seen in spectral density $S(\omega)$ of the wavefunction $\psi_x(t)$. This density is defined as: $S(\omega) = \sum_x |a_x(\omega)|^2$, where $a_x(\omega) = \sum_{t=0}^{T_f} \psi_x(t) \exp(i\omega t)/\sqrt{T_f}$ and T_f is a large time scale on which the spectrum is determined (we usually used $T_f \approx 5T_G \gg T_G$). The phase diagram of spectral density $S(\omega)$ dependence on the imperfection strength ε is shown in Figure 3. Two phases are clearly seen: for $\varepsilon < \varepsilon_c$ the diagram contains four lines corresponding to the four states (3), while for $\varepsilon > \varepsilon_c$ these lines are destroyed and the spectrum becomes continuous. These phases correspond to the qualitative change of the Husimi distribution shown in Figure 2.

To study the transition between these phases in a more quantitative way we analyze the dependence of probabilities w_G and w_4 on the imperfection strength ε for a large number of disorder realizations in H_S (2) changing also the number of qubits n_{tot}. The number of realizations vary from 50 to 1000 depending on ε and n_{tot}. Since the frequency of Grover oscillations varies strongly with ε and disorder we average w_G and w_4 over a large time interval T_f to suppress fluctuations in time. The obtained results are summarized in Figure 4. For a fixed value of n_{tot} the dependence $w_G(\varepsilon)$ changes strongly from one realization to another (Fig. 4a). In contrast, the probability w_4 remains close to unity being insensitive to variations of disorder up to $\varepsilon < \varepsilon_c$ (Fig. 4b). Only for $\varepsilon > \varepsilon_c$, when $w_4 \ll 1$, it becomes sensitive to disorder. The probabilities averaged over disorder $\bar{w}_G$ and $\bar{w}_4$ are shown in Figures 4a and 4b. They also have a qualitative change in behavior near ε_c, especially $\bar{w}_4$. The two phases are clearly seen from the data of Figure 4: at $\varepsilon < \varepsilon_c$ the 4-states approximation is valid and for $\varepsilon > \varepsilon_c$ a transition to chaos mixing takes place. In the regime $\varepsilon < \varepsilon_c$ the probability to find system in the searched state can be close to unity for $\varepsilon \sim \omega_G$ or much smaller than unity for $\omega_G \ll \varepsilon \ll \varepsilon_c$, however the 4-states approximation remains valid up to $\varepsilon \approx \varepsilon_c$. These results confirm the fact that the phase transition takes place near some critical ε_c for an ensemble of disorder realizations.

The value of ε_c can be obtained from the following estimate. The transition rate induced by imperfections after one Grover iteration is given by the Fermi golden rule: $\Gamma \sim \varepsilon^2 n_g^2 n_{tot}$, where n_{tot} appears due to random contribution of qubit couplings ε while n_g^2 factor takes into account coherent accumulation of perturbation on n_g gates used in one iteration (see, e.g. [10]). In the Grover algorithm the four states (3) are separated from all other states by energy gap $\Delta E \sim 1$ (it appears due to sign change introduced by operators O and D). Thus these four states become mixed with all others for

$$\varepsilon > \varepsilon_c \approx 1.7/(n_g\sqrt{n_{tot}}) \qquad (4)$$

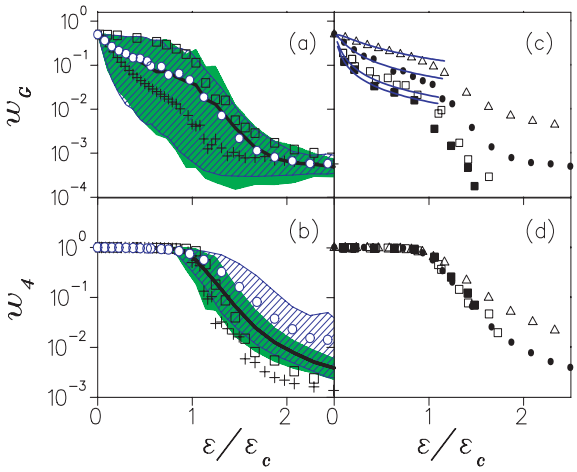

Fig. 4. Dependence of probabilities w_G (a, c) and w_4 (b, d) on rescaled imperfection strength $\varepsilon/\varepsilon_c$, with ε_c from (4). For panels (a, b) $n_{tot} = 12$, squares and pluses show data for two typical disorder realizations, green/grey area shows the region of probability variation for various disorder realizations (see text), full thick curves give average dependence $\bar{w}_G$, $\bar{w}_4$. Dashed area bounded by thin curves show the region of probability variation in the single-kick model, open circles give the average data in this model with rescaling factor $R = 0.56$. Panels (c, d) show $\bar{w}_G$, $\bar{w}_4$ for $n_{tot} = 9$ (triangles), 12 (full circles), 15 (open squares) and 16 (full squares). In panel (c) full curves are given by equation (6) for same n_{tot} values from top to bottom, $R = 0.56$. A color version is available online at `http://www.eurphysj.org`.

when $\Gamma > \Delta E$. Here the numerical factor is obtained from numerical data. The parameter dependence is well confirmed by data for $\bar{w}_4$ shown in Figure 4d.

The variation of averaged Grover probability $\bar{w}_G$ with ε and n_{tot} is presented in Figure 4c. The dependence on system parameters can be understood on the basis of simple single-kick model. In this model the action of static imperfections in all gates entering in one Grover iteration is replaced by a single kick unitary operator $U_{eff} = \exp(-iH_S n_g R)$ acting after each iteration. Here R is a dimensionless renormalization factor which takes into account that gates do not commute with H_S. Figures 4a and 4b show that this single kick approximation gives a good description of original averaged data with $R = 0.56$. Thus, the renormalization effects play a significant role and therefore this model does not describe the probability variation for a given disorder realization. However, the averaged dependence is correctly reproduced. It is interesting to note that the single kick approximation gives also a qualitatively correct description of time scale for fidelity decay in the quantum tent map discussed in [10] (see e.g. Eq. (49) there: here a quadratic dependence on n_g is similar to the effect of single kick approximation).

In the regime where the dynamics of Grover algorithm is dominated by four states subspace (3) the single-kick model can be treated analytically. The matrix elements of the effective Hamiltonian in this space are

$$H_{eff} = \begin{pmatrix} A+a & 0 & -i\omega_G & 0 \\ 0 & A-a & 0 & -i\omega_G \\ i\omega_G & 0 & B & b \\ 0 & i\omega_G & b & B \end{pmatrix}, \qquad (5)$$

where $A = -Rn_g \sum_{i=1}^{n_q} a_i \langle\tau|\sigma_i^{(z)}|\tau\rangle$, $B = Rn_g \sum_{i<j}^{n_q} b_{i,j} - b$, $a = -Rn_g a_{n_q+1}$ and $b = Rn_g(b_{n_q+1,n_q+2-L_x} + b_{n_q+1,L_x} + b_{n_q,n_q+1} + b_{n_q+1-L_x,n_q+1})$ and qubits are arranged on $L_x \times L_y$ lattice, and numerated as $i = x + L_x(y-1)$, with $x = 1, \ldots, L_x$, $y = 1, \ldots, L_y$. In the limit of large n_q the terms a, b are small compared to A, B by a factor $1/\sqrt{n_q}$ and H_{eff} is reduced to 2×2 matrix, which gives $w_G = 2\omega_G^2/[(A-B)^2 + 4\omega_G^2]$. For large n_q the difference $A - B$ has a Gaussian distribution with width $\sigma = Rn_g\sqrt{n_q/3}\sqrt{\alpha^2 + 2\beta^2} = \varepsilon Rn_g\sqrt{n_q}$. The convolution of w_G with this distribution gives

$$\bar{w}_G = \sqrt{\pi/2}(1 - \mathrm{erf}(\sqrt{2}\omega_G/\sigma)) \exp(2\omega_G^2/\sigma^2)\, \omega_G/\sigma. \quad (6)$$

This formula gives a good description of numerical data in Figure 4c that confirms the validity of single-kick model. For $\sigma \gg \omega_G$ and a typical disorder realization with $(A-B) \sim \sigma$ the actual frequency of Grover oscillations is strongly renormalized: $\omega \approx (A-B) \sim \sigma \gg \omega_G$, and in agreement with Figure 3 $\omega \sim \varepsilon/\varepsilon_c$. In this typical case $w_G \sim \omega_G^2/\sigma^2 \ll 1$ (almost total probability is in the states $|\eta_0\rangle$, $|\eta_1\rangle$). Hence, the total number of quantum operations N_{op}, required for detection of searched state $|\tau\rangle$, can be estimated as $N_{op} \sim N_M/\omega \sim \sigma/\omega_G^2 \sim \varepsilon N/\varepsilon_c$, where $N_M \sim 1/w_G \sim \sigma^2/\omega_G^2$ is a number of measurements required for detection of searched state [20]. Thus, in presence of strong static imperfections the parametric efficiency gain of the Grover algorithm compared to classical one is of the order $\varepsilon_c/\varepsilon$. For $\varepsilon \sim \omega_G$ the efficiency is comparable with that of the ideal Grover algorithm while for $\varepsilon \sim \varepsilon_c$ there is no gain compared to the classical case.

It is interesting to make comparison with the case of random errors in quantum gates discussed in [7]. In this case the probability w_G drops exponentially with the number of gates and becomes very small after the time $\pi/2\omega_G$: $w_G \sim \exp(-\pi\varepsilon^2 n_g/(2\omega_G)) \sim 1/N$. Thus for random errors the quantum algorithm looses its efficiency for $\varepsilon \sim (\omega_G/n_g)^{1/2} \ll \varepsilon_c$ [21]. As a result we conclude that the Grover algorithm is robust with respect to static imperfections but it is sensitive to random errors in quantum gates. The later fact is related to the quadratic speedup of the Grover algorithm.

In summary, we have shown that the Grover algorithm remains robust against static imperfections inside a well defined domain and determined the dependence of algorithm efficiency on the imperfection strength.

This work was supported in part by the EU IST-FET project EDIQIP, by the NSA and ARDA under ARO contract No. DAAD19-01-1-0553, and by the French government ACI (Action Concertée Incitative) Nanosciences-Nanotechnologies LOGIQUANT. We thank IDRIS at Orsay and CalMip at Toulouse for access to their supercomputers.

References

1. M.A. Nielsen, I.L. Chuang, *Quantum Computation and Quantum Information* (Cambridge Univ. Press, Cambridge, 2000)
2. P.W. Shor, in *Proceedings of the 35th Annual Simposium on Foundation of Computer Science*, edited by S. Goldwasser (IEEE Computer Society, Los Alamos, CA, 1994), p. 124.
3. L.K. Grover, Phys. Rev. Lett. **79**, 325 (1997)
4. J.I. Cirac, P. Zoller, Phys. Rev. Lett. **74**, 4091 (1995)
5. C. Miguel, J.P. Paz, W.H. Zurek, Phys. Rev. Lett. **78**, 3971 (1997)
6. B. Georgeot, D.L. Shepelyansky, Phys. Rev. Lett. **86**, 5393 (2001)
7. P.H. Song, I. Kim, Eur. Phys. J. D **23**, 299 (2003)
8. M. Terraneo, D.L. Shepelyansky, Phys. Rev. Lett. **90**, 257902 (2003)
9. S. Bettelli, Phys. Rev. A **69**, 042310 (2004)
10. K.M. Frahm, R. Fleckinger, D.L. Shepelyansky, Eur. Phys. J. D **29**, 139 (2004)
11. B. Georgeot, D.L. Shepelyansky, Phys. Rev. E **62**, 3504 (2000); Phys. Rev. E **62**, 6366 (2000)
12. G.P. Berman, F. Borgonovi, F.M. Izrailev, V.I. Tsifrinovich, Phys. Rev. E **64**, 056226 (2001)
13. G. Benenti, G. Casati, D.L. Shepelyansky, Eur. Phys. J. D **17**, 265 (2001)
14. G. Benenti, G. Casati, S. Montangero, D.L. Shepelaynsky, Phys. Rev. Lett. **87**, 227901 (2001)
15. A.A. Pomeransky, D.L. Shepelaynsky, Phys. Rev. A **69**, 014302 (2004)
16. D. Braun, Phys. Rev. A **65**, 042317 (2002)
17. A. Barenco et al., Phys. Rev. A **52**, 3457 (1995)
18. C. Miquel, J.P. Paz, M. Saraceno, Phys. Rev. A **65**, 062309 (2002)
19. S.-J. Chang, K.-J. Shi, Phys. Rev. A **34**, 7 (1986)
20. Here we consider only the subspace (3), a small probability leakage to all other states is not crucial since it will be randomly distributed over $2N-4$ states
21. Some improvement can be reached in this situation if to perform measurements after a shorter number of iterations given by a typical decay time $t_{dec} \sim 1/(\varepsilon^2 n_g) \ll 1/\omega_G$ Then the search probability is small but multiple repetitions of the algorithm allow to detect the searched state after a number of quantum operations $N_{op} \sim t_{dec} n_g / w_G$ where the probability of searched state is $w_G \sim t_{dec}^2/N$. The number of quantum operations for this strategy is $N_{op} \sim (\varepsilon n_g)^2 N$